Chemosphere 373 (2025) 144127

Contents lists available at ScienceDirect

Chemosphere

journal homepage: www.elsevier.com/locate/chemosphere

ANN-assisted comprehensive screening of silica gel-alunite composite sorbent system for efficient adsorption of toxic nickel ions: Batch and continuous mode water treatment applications

Sibel Tunali Akar [a,*], Suzan Rüstemoğlu [b], Serpil Turkyilmaz [c], Fatih Sayin [a], Tamer Akar [a]

[a] Eskişehir Osmangazi University, Faculty of Science, Department of Chemistry, 26040, Eskişehir, Turkey
[b] Eskişehir Osmangazi University, Graduate School of Natural and Applied Sciences, Department of Chemistry, 26040, Eskişehir, Turkey
[c] Bilecik Şeyh Edebali University, Faculty of Science, Department of Statistics and Computer Sciences, 11230, Bilecik, Turkey

HIGHLIGHTS

- Sg@Aln was successfully employed for Ni^{2+} sorption in both batch and column systems.
- Sg@Aln showed excellent Ni^{2+} sorption performance in real wastewater.
- ANN has the best prediction capability for optimum removal efficacy.
- The maximum Ni^{2+} removal by Sg@Aln reached up to 89.11%.

GRAPHICAL ABSTRACT

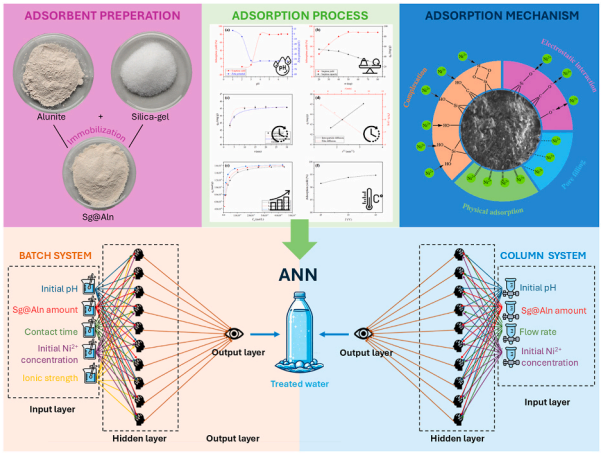

ARTICLE INFO

Handling editor: Yongmei Li

Keywords:
Adsorption
Alunite
Artificial neural networks
Immobilization
Nickel
Silica-gel

ABSTRACT

Through batch and fixed-bed column operations, nickel ions were extracted from a contaminated aqueous media by adsorption onto silica gel-immobilized alunite (Sg@Aln). A three-layer backward-propagating network with an ideal pattern of 5-10-1 and 4-10-1 was used to train and validate an artificial neural network (ANN) model for process modeling and optimization in batch and continuous systems, respectively. For the test dataset, the model outputs of the model pointed out a satisfactory alignment between the anticipated and experimental response. The Sg@Aln dosage and contact time were recorded as the most relevant parameters in Ni^{2+} elimination. The Sg@Aln-metal interactions were also characterized using a variety of instrumental approaches. The maximum Ni^{2+} adsorption was achieved by utilizing 2 g/L of the adsorbent at a solution pH of 5.0 after 10 min of contact time, equating to 89.11%. The data corresponded well with the non-linear shape of the Langmuir isotherm (R^2 = 0.99), and the computed maximal adsorption capacity was 96.01 mg/g (1.64×10^{-3} mol/g) at 25 °C. Kinetic

* Corresponding author.
E-mail address: stunali@ogu.edu.tr (S. Tunali Akar).

https://doi.org/10.1016/j.chemosphere.2025.144127
Received 5 August 2024; Received in revised form 17 December 2024; Accepted 14 January 2025
Available online 31 January 2025

analysis reveals that the adsorption process is consistent with the pseudo-second-order model, with $R^2 = 0.9998$. Thermodynamic findings indicated endothermicity, spontaneity, and adsorption favorability. Sg@Aln could remove 41.23 mg/g and 33.20 mg/g of Ni^{2+} from actual wastewater in batch and continuous processes, respectively. While the Sg@Aln column's breakthrough curve is consistent with Chu's simplistic model, the breakthrough capacity was 69.35 mg/g. Overall, the results might open new possibilities for treating metal pollution in the aquatic environment.

1. Introduction

Because of their poisonous nature and propensity to bioaccumulate in the food chain, heavy metals are a serious environmental problem even at very low concentrations. Because heavy metals tend to bioaccumulate in the food chain, even in minimal quantities, their presence in the environment is a serious problem. Heavy metal-contaminated water can cause significant health problems for humans if discharged into the environment without being adequately treated as soon as possible (Ali et al., 2019). One such heavy metal that is usually found in wastewater is nickel. It greatly contributes to environmental contamination because of its extensive use in nickel mining, storage batteries, stainless steel, pigment manufacturing, tannery, and electroplating industries (Raval et al., 2016; El-Naggar et al., 2021).

While it can exist in various oxidation states, +2 is the most common oxidation state in the environment. Significant toxic consequences are unavoidable at high doses of Ni^{2+}, even though it has a trace element function that can activate a specific enzyme system in small quantities. Toxic nickel ions can dissolve in water, reach the food chain, and endanger human health. Humans might suffer from a range of pathological outcomes, from contact dermatitis to lung fibrosis, kidney, and cardiovascular disorders, and even cancer if they are exposed to extremely Ni-polluted sources (Denkhaus and Salnikow, 2002; Kasprzak et al., 2003). Nickel poisoning primarily affects the lungs, immunological system, and respiratory tract through occupational inhalation exposure. Exposure through inhalation can potentially impact non-occupational people. Human exposure mainly occurs through oral intake of food and water because nickel can be harmful in both (Genchi et al., 2020). According to WHO-recommended standards, drinking water can contain no more than 0.07 mg/L of nickel (WHO, 2022). As a result, removing nickel from contaminated waters is a critical issue that requires research. For metal-containing wastewaters are currently treated using a variety of standard procedures, including reverse osmosis, electrochemical treatment, chemical precipitation, oxidation/reduction, filtration, and ion exchange. However, their extensive application is occasionally limited due to technological and cost constraints (Volesky, 2001). It is essential to control metal pollution in water by developing practical and efficient approaches to support or suggest alternatives to current treatment procedures.

Adsorption is a valuable water treatment technique for the removal of hazardous contaminants from water and wastewater due to some important advantages such as simplicity, practicability, cost-efficiency, eco-friendly etc., which are of primary importance for the efficient removal of contaminants from the aqueous medium (Tripathi and Ranjan, 2015; Alahabadi et al., 2020) Thus, numerous low-cost and widely available raw materials have been studied as potential adsorbents for the removal of harmful metal pollutants from contaminated water (Anastopoulos et al., 2019; Bilal et al., 2021). Surface modifications, on the other hand, are strategies for improving adsorbent materials' adsorption characteristics and efficacy. The resulting designed sorbent materials may be considered more suitable for practical applications.

In this context, research has concentrated on increasing the pollutant removal potential of sorbent materials using approaches including physical and chemical pre-treatment (Foroutan et al., 2018; Bosacka et al., 2022; Raninga et al., 2023), impregnation (Natrayan et al., 2022; Shahryari et al., 2022), and surface coating (Ahmaruzzaman, 2011; Akar et al., 2013; Natrayan et al., 2022; Amin et al., 2023; Mondal et al., 2024).

Adsorptive treatment is a complicated process in which multiple variables might act concurrently. Modeling any system or process is a difficult and important endeavor in engineering. The difficulty might be attributed to the physical complexity of natural processes or inability of mathematical expertise. Machine Learning (ML) is a strong tool in helping solve such obstacles by developing basic models from observable patterns and supporting decision-makers in solving real-world challenges. ML techniques are gaining popularity among engineers because they can map causal factors and outcomes from observed patterns in experimental data, without requiring deep knowledge of the complex physical processes involved (Ahmad Aftab et al., 2023). The most recent advances in mathematical modeling include employing artificial neural networks (ANN). Recent achievements in mathematical modeling involve employing ANN, which mimics biological networks of neurons by implementing nonlinear functions. Using ANN in process modeling is a creative approximation, eliminating the need for elaborate analytical process explanations. Thus, a model-free process simulator is created by exposing the network to representative process samples. The number of publications devoted to applying ANN in process and chemical engineering demonstrates an increasing interest in it (Tomczak, 2011; Ghaedi and Vafaei, 2017; Choi et al., 2022).

Alunite, with the chemical formula $KAl_3(SO_4)_2(OH)_6$, is an intriguing natural mineral that may be used to make aluminum sulfate, alumina, potassium alum, sulfuric acid, coagulant, elemental sulfur, potassium sulfate, and quartz sand. A small number of research on the use of alunite as an adsorbent for various contaminants has presented remarkable results (Tunali Akar et al., 2023).

To generate an efficient, and environmentally acceptable composite adsorbent material for the removal of Ni^{2+} ions, the powder of alunite was immobilized with silica gel employing a simple immobilization process. In this context, the present work proposes a new study approach for exploring the adsorption characteristics of adsorbent surfaces, with an emphasis on optimizing Ni^{2+} adsorption via a composite of silica-gel and alunite (Sg@Aln). This study addresses a gap in the literature by examining the synergistic effects of silica-gel and alunite materials for the adsorption process. The innovation of this study relies not only on the design of a new modified sorbent (Sg@Aln) but also on the optimization of several parameters (both batch and continuous mode parameters) for Ni^{2+} adsorption by ANN to acquire useful data for the construction of the water treatment model. This coordinated approach improves environmental remediation operations.

To further understand the Ni^{2+} removal process, kinetics, isotherm, and thermodynamic investigations were conducted in addition to instrumental characterization studies. Sg@Aln was tested for Ni^{2+} uptake from an industrial effluent and a breakthrough study is being conducted to ascertain the practical use of the method. Overall, we offer an ecologically friendly approach for effectively cleaning nickel-contaminated water, contributing to a more sustainable environment.

2. Materials and methods

2.1. Immobilized sorbent

Alunite was utilized to prepare the immobilized sorbent and was supplied by Kütahya-Şaphane, Turkey. An immobilization procedure

that Lopez et al. had previously reported was applied with some modifications (López et al., 1997). 10 g of silica gel (Sigma-Aldrich, 28–200 mesh, grade 12) was dissolved by heating in a solution of potassium hydroxide (Merck, 85%) at a concentration of 7% (w/v). 100 mL of a suspension consisting of 5 g of alunite in deionized water was added when the temperature had decreased to 20 °C and well stirred. Phosphoric acid (Riedel de Haen, 85%) solution (20% v/v) was added in a certain amount to provide the gel to form. The resultant gel was employed as an adsorbent material in the powdered form of Sg@Aln after being dried at 80 °C in an oven for an entire night. The nickel adsorption capacity of blank silica gel was assessed after it was made similarly without using alunite.

2.2. Chemicals and instruments used

Stock solutions were prepared using $Ni(NO_3)_2.6H_2O$ (≥97.0%), acquired from Sigma Aldrich. Various concentrations of Ni^{2+} ion solutions were produced by carefully diluting these solutions. The pH levels of the liquids were altered by diluted NaOH (Merck, 99%) and HNO_3 (Merck, 65%) solutions. WTW Inolab pHmeter was used for pH measurement in this investigation. Before and after the adsorption tests, the concentration of Ni^{2+} in the supernatant solutions was detected using a PerkinElmer AAnalyst 400, FAAS, Atomic Absorption Spectrophotometer. A Malvern zetasizer was used to determine zeta potentials to investigate surface charges at different pH levels. Sg@Aln's surface area was measured using a Quantachrome Instruments Autosorb 1 type BET surface area analyzer. SEM (Hitachi Regulus 8230 FE-SEM) at 10 keV accelerating voltage was used to examine the surface morphology of Sg@Aln. A PerkinElmer STA 8000 DTA/TG device was used to study the thermal characteristics of the adsorbent. PerkinElmer Spectrum Two FTIR spectrophotometer was used to obtain FTIR spectra to determine the functional groups present on the sorbent material's surface.

2.3. Batch adsorption studies

To examine the adsorption characteristics of Ni^{2+} by Sg@Aln in 25 mL aqueous solutions, a batch adsorption procedure was used. Batch adsorption studies were conducted by varying the pH (2–7), sorbent dosage (20–80 mg), contact period (3–30 min), and ionic strength (0.01–0.1 M) to find the best experimental conditions. A Thermo Variomag Poly 15 was employed for mixing the Ni^{2+} ion solutions at room temperature and 250 rpm while adding a known amount of Sg@Aln. Using a centrifuge, the Sg@Aln was separated from the liquid phase. Then, the resulting solutions were quantified by FAAS concerning Ni^{2+} ions. The following formula is used to determine the adsorbent's adsorption capacity (q_e, mg/g).

$$q_e = \frac{V(C_i - C_e)}{m} \quad (1)$$

where, C_i and C_e represent, respectively, the Ni^{2+} ion concentrations (mg/L) in the solution before and after the Ni^{2+} adsorption tests. V is the Ni^{2+} solution volume (L), and m is the Sg@Aln amount (g).

This study examined adsorption isotherms using different initial metal ion concentrations ranging from 100 to 400 mg/L with 50 mg of Sg@Aln. MINTEQ 4.0 software was used to analyze nickel species and the results indicated that Ni^{2+} ions at a concentration of 400 mg/L do not precipitate or transform into any other species (Fig. S2). The kinetic experiments were performed with a fixed initial Ni^{2+} ion concentration of 100 mg/L and varying contact times from 3 to 30 min. Each trial in the present research was done at least three times and average results were presented. SPSS 17.0 version was used to evaluate the data statistically.

2.4. Ni^{2+} adsorption studies in continuous mode

A 10.5 mm i.d. glass column for sorbent filling, an Ismatec Ecoline IP16 peristaltic pump for solution flow, and Tygon tubing for connecting made up the continuous-mode adsorption system used in this work. The concentration of the Ni^{2+} ion solution was maintained as it was pumped through the column in an up-flow mode. After the adsorption process, effluents were collected and analyzed for Ni^{2+} ions.

2.5. ANN modeling

ANN approach has been effectively used in recent decades as an alternate modeling strategy to simulate the nonlinear interactions present in complicated chemical reactions like adsorption. It can be appropriately used for heavy metal removal to identify the non-linear correlations between operating parameters in wastewater treatment processes (Mandal et al., 2015). The model's correctness in characterizing the prepared adsorbent's adsorption efficiency has been demonstrated by comparing the findings of the experimental and statistical models. Computational intelligence approaches for classification of medical data: State-of-the-art, future challenges, and research directions (Kalantari et al., 2018). It is based on the biological nervous system of humans and can manage input and output and establish linear relationships between model parameters. Artificial neurons, also known as artificial nodes, are basic factors in this multi-layer architecture that may be used to calculate and produce output datasets for input dataset variables. There are various ways to apply these fundamental processing parameters to create the structure of a neural network (Zhang et al., 2024).

In this research, the functional relationship between the operational conditions and the equilibrium adsorption capacity of Sg@Aln for the Ni^{2+} removal is characterized by ANN models through the NN toolbox of the MATLAB 2021a software. The ANN was used to import the adsorption dataset, which was collected from experiments on how environmental conditions affected Ni^{2+} removal in both batch and column systems. The Levenberg-Marquardt (LM) approach was chosen to train the ANN because of its superior efficacy (Vinayagam et al., 2024). There were three layers, 5 input layers, 1 hidden layer with 10 neurons, and 1 output layer for the batch system, and 4 input layers were used for the column system (Fig. S1). Data points were randomly grouped into three separate sets: 75% for training, 15% for validation, and 10% for testing.

The mean square error (MSE) (Eq. (2)) assesses the predictive performance of the regression model , whereas the regression coefficient (R) (Eq. (3)) evaluates the linear correlation and direction between input variables and output. These two statistical parameters are commonly used to evaluate the effectiveness of ANN models and are calculated as follows (Yousefi et al., 2024):

$$MSE = \sqrt{\frac{1}{N}\sum_{i=1}^{n}(act_i - pre_i)^2} \quad (2)$$

$$R^2 = \left(\frac{\sum_{i=1}^{n}(act_i - \overline{act})(pre_i - \overline{pre})}{\sum_{i=1}^{n}(act_i - \overline{act})^2 \sum_{i=1}^{n}(pre_i - \overline{pre})^2} \right)^2 \quad (3)$$

3. Results and discussion

3.1. pH effect

The adsorption process can be affected by the ionized forms of the heavy metal ions as well as the surface characteristics of the sorbent material. Fig. 1a displays the study of pH values ranging from 2.0 to 7.0 on the adsorption of Ni^{2+}. Ni^{2+} adsorption on Sg@Aln was significantly affected by medium pH values. All of the nickel species in the studied pH range were determined to be in the form of Ni^{2+} ions using MINTEQ 4.0 software (Fig. S2). Because of the electrostatic repulsive forces between

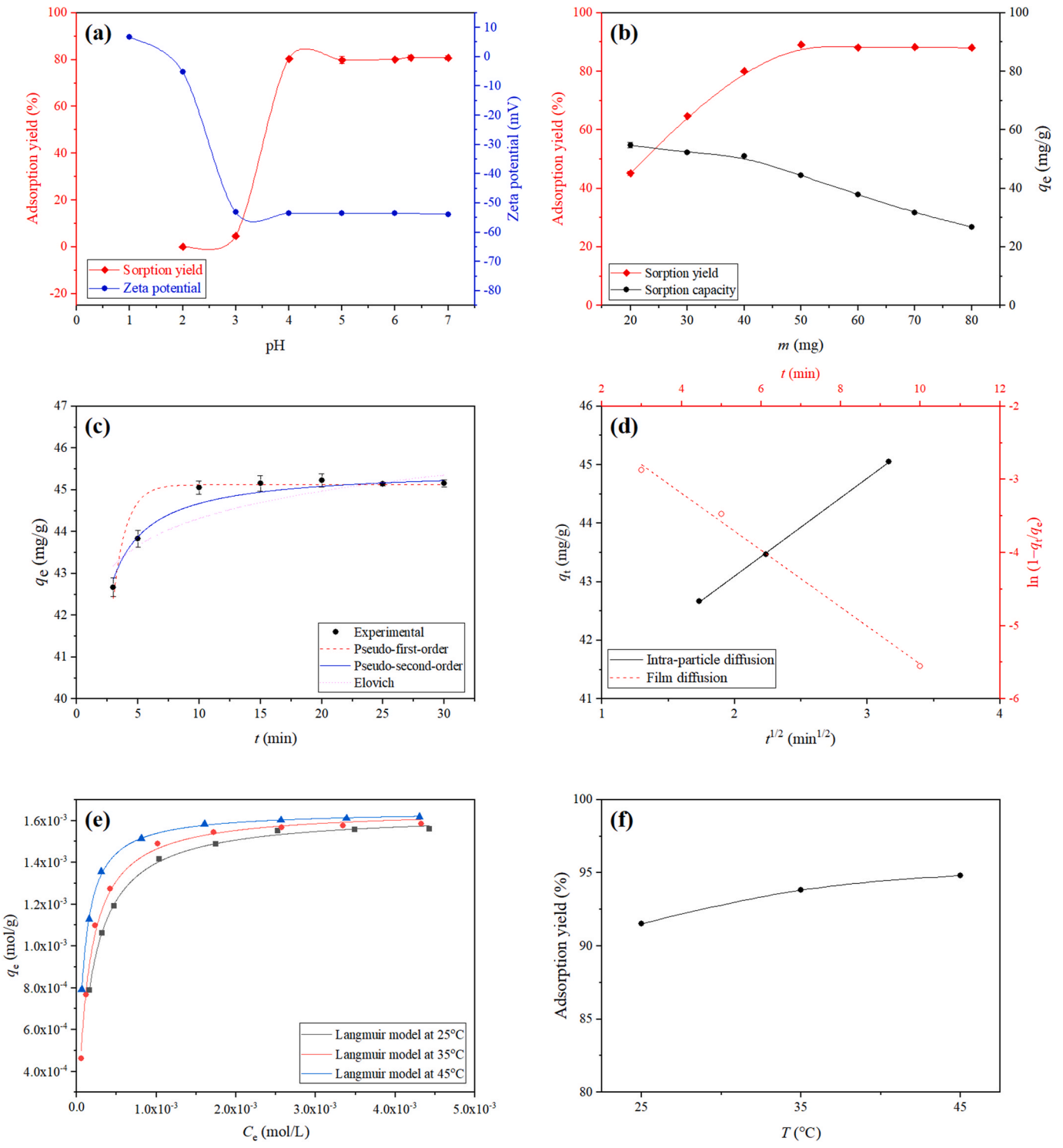

Fig. 1. Effect of pH on the Ni^{2+} adsorption by Sg@Aln and zeta potential of Sg@Aln (m: 40 mg, V: 25 mL, t: 60 min, C_0: 100 mg/L, T: 25 °C) **(a)** Effect of adsorbent dosage on the Ni^{2+} adsorption by Sg@Aln (pH: 5.0, V: 25 mL, t: 60 min, C_0: 100 mg/L, T: 25 °C) **(b)**. Time-dependent data and adsorption kinetics for Ni^{2+} adsorption by Sg@Aln (pH: 5.0, m: 50 mg, V: 25 mL, C_0: 100 mg/L, T: 25 °C) **(c).** Particle and intra-particle diffusion models for Ni^{2+} adsorption by Sg@Aln **(d)**. Effect of initial Ni^{2+} concentration on the adsorption capacity of Sg@Aln and Ni^{2+} adsorption isotherm models (pH: 5.0, m: 50 mg, V: 25 mL, t: 10 min, T: 25 °C) **(e)** and effect of temperature on the Ni^{2+} adsorption by Sg@Aln (pH: 5.0, m: 50 mg, C_0: 100 mg/L, V: 25 mL, t: 10 min) **(f)**.

the H_3O^+ and Ni^{2+} ions, no metal adsorption occurred under strongly acidic conditions (at pH 2.0 and 3.0). Another reason why adsorption does not occur at low pH values might be competition between increased protons and Ni^{2+} ion concentrations. The highest removal of Ni^{2+} ions was then accomplished with an adsorption yield of 80.29% at about pH 4.0. The Ni^{2+} adsorption trend on Sg@Aln could also be explained by pH-dependent sorbent surface charge (Fig. 1a). The values of zero point of charge (ZPC) of alunite and Sg@Aln were found to be 4.1 (Tunali Akar et al., 2023) and 1.7 , respectively. Both adsorbent surfaces were positively charged at pH values lower than ZPC and Sg@Aln surface had a higher positive value than alunite in the investigated pH range. This may be an important reason for the higher adsorption performance of

Sg@Aln than alunite. At pH > 1.7, increased Ni^{2+} adsorption yield was due to the adsorbent's surface having a large amount of negative charge.

3.2. Effect of Sg@Aln dosage

Fig. 1b indicated that the removal yields of Ni^{2+} ions steadily increased from 45.27% to 89.11% with increasing Sg@Aln mass from 20 mg to 50 mg. Higher doses of adsorbent result in more active binding sites, which raises the adsorption yield. Afterward, the adsorption yield of Ni^{2+} ions on the Sg@Aln stayed constant due to the saturation of active sites on the sorbent surface. Therefore, 50 mg was selected to minimize Sg@Aln dose and maximize Ni^{2+} uptake.

3.3. Effect of time

The impact of contact time, with periods varying from 3 to 30 min, on the performance of Ni^{2+} adsorption was investigated at room temperature. Within the first 10 min of the adsorption procedure, Ni^{2+} ions quickly adsorb onto Sg@Aln, as shown in Fig. 1c. Moreover, the adsorption equilibrium for Ni^{2+} was rapidly reached in less than 10 min. This result suggested that Sg@Aln might be used effectively for the fast treatment of metal-contaminated wastewater.

3.4. Adsorption kinetics

The adsorption kinetics was investigated using the pseudo-first-order (Eq. S(1)) (Lagergren, 1889), the pseudo-second-order (Eq. S(2)) (Ho and McKay, 1999), Elovich (Eq. S(3)), film diffusion model (Eq. S(4)) (Boyd et al., 1947), and intra-particle diffusion model (Eq. S(5)) (Weber and Morris, 1963) to evaluate the rate of adsorption and mechanism for Ni^{2+} adsorption onto Sg@Aln. Model equations and related explanations are presented in supplementary information (Section S1).

The pseudo-second-order model demonstrated excellent linearity, having a coefficient of determination (0.999) for the adsorption of Ni^{2+} ions onto Sg@Aln. The model parameters are presented in Table 1. The adsorption capacity determined using the model equation agrees with the value obtained from the experiments. On the other hand, due to a lower R^2 value and inconsistent experimental and computed values of q_e, it was determined that the pseudo-first-order kinetic model did not sufficiently explain the time-dependent data. In addition, the experimental kinetic results do not follow Elovich kinetics, suggesting that the surface is not energetically heterogeneous.

Film diffusion and intra-particle diffusion models were also tested to examine the contributions of both processes to the adsorption of Ni^{2+} by Sg@Aln (Fig. 1d). A linear curve in the graphs of q_t vs. $t^{1/2}$ and ln (1- q_t/q_e) vs. t for the data until equilibrium indicate that the rate-limiting phase (the slowest step) may be film diffusion or intraparticle diffusion. However, the presence of nonzero intercepts in the plots suggests that the adsorption kinetics may be sequentially influenced by both film diffusion and intra-particle diffusion by multiple mechanisms (Sivasankar et al., 2012; Dharmarathna and Priyantha, 2024).

Table 1
Kinetic parameters for Ni^{2+} adsorption onto Sg@Aln.

Pseudo-first-order	k_1 (1/min)	q_e (mg/g)	R^2
	0.94 ± 0.05	45.12 ± 0.07	0.871
Pseudo-second-order	k_2 (g/mg min)	q_e (mg/g)	R^2
	0.12 ± 0.01	45.50 ± 0.07	0.938
Elovich	α (mg/g min)	β (g/mg)	R^2
	$(2.34 \pm 0.25) \times 10^{19}$	1.06 ± 0.24	0.729
Film diffusion	k_{FD} (1/min)	n	R^2
	1.63 ± 0.17	−0.39 ± 0.03	0.996
Intra-particle diffusion	k_{IPD} (mg/g min^2)	C (mg/g)	R^2
	1.67 ± 0.04	39.79 ± 0.09	0.999

3.5. Equilibrium isotherms

The non-linear regression fitting of Freundlich (1906), Langmuir (1918), D-R (Dubinin and Radushkevich, 1947) and Elovich (Elovich and Larinov, 1962) isotherms was used in the present research to assess the equilibrium adsorption data and these models were described in Section S2 (Supplementary information, Eqs. S6-S9). The adsorption data of Ni^{2+} onto Sg@Aln better fitted the Langmuir model (Fig. 1e) with the R^2 value of 0.99 (Table 2). This finding implied that the adsorption of Ni^{2+} ions onto Sg@Aln followed a monolayer adsorption process. The maximum monolayer Ni^{2+} adsorption capacity value of Sg@Aln was 1.64×10^{-3} mol/g (96.01 mg/g) at 25 °C. Table S1 indicates the maximum Ni^{2+} adsorption capacity of Sg@Aln is higher than that of other adsorbents. E value suggested that the adsorption of Ni^{2+} ions onto Sg@Aln may involve chemical adsorption.

3.6. Temperature effect and thermodynamics of Ni^{2+} adsorption onto Sg@Aln

The impact of temperature on Ni^{2+} adsorption was examined at temperatures ranging from 25 to 45 °C. According to the findings (Fig. 1f), increasing temperature causes an increase in Ni^{2+} adsorption yield of immobilized alunite, which indicates an endothermic process. Sg@Aln has a high adsorption yield at all temperatures investigated, which may be regarded as an essential benefit for the treatment of wastewater applications. Thermodynamic parameters (ΔG°, ΔH°, and ΔS°) were computed from the slope and intercept of the Van't Hoff plot (Fig. S3), as described in Eqs. 4-6:

$$K = K_L \times 55.5 \quad (4)$$

$$\Delta G^\circ = -RT \ln K_L \quad (5)$$

$$\Delta G^\circ = \Delta H^\circ - T\Delta S^\circ \quad (6)$$

where, ΔG° (kJ/mol) is the standard free energy, ΔH° (kJ/mol) is the standard enthalpy change, ΔS° (kJ/mol) is the standard entropy change, T (K) is the absolute temperature, and R (8.314 J/mol K) is the ideal gas constant (Lima et al., 2019).

Table 2
Isotherm parameters for Ni^{2+} adsorption onto Sg@Aln.

Langmuir	T (°C)	q_m (mol/g)	K_L (L/mol)	R^2
	25	$(1.64 \pm 0.07) \times 10^{-3}$	$(5.85 \pm 0.14) \times 10^{3}$	0.998
	35	$(1.65 \pm 0.15) \times 10^{-3}$	$(7.67 \pm 0.37) \times 10^{3}$	0.996
	45	$(1.65 \pm 0.05) \times 10^{-3}$	$(1.42 \pm 0.03) \times 10^{4}$	0.999
Freundlich	T (°C)	n	K_F $((mol\ g^{-1})\ (mol\ L^{-1}))^{1/n}$	R^2
	25	5.88 ± 0.90	$(4.18 \pm 0.70) \times 10^{-3}$	0.897
	35	5.14 ± 0.95	$(5.00 \pm 1.19) \times 10^{-3}$	0.849
	45	7.71 ± 1.47	$(3.48 \pm 0.58) \times 10^{-3}$	0.823
D–R	T (°C)	q_m (mol/g)	E (kJ/mol)	R^2
	25	$(2.38 \pm 0.17) \times 10^{-4}$	15.58 ± 1.96	0.928
	35	$(2.57 \pm 0.26) \times 10^{-4}$	14.93 ± 2.34	0.893
	45	$(2.23 \pm 0.15) \times 10^{-4}$	18.32 ± 2.89	0.894
Elovich	T (°C)	q_m (mol/g)	K_E (L/mol)	R^2
	25	$(3.09 \pm 0.44) \times 10^{-4}$	$(1.45 \pm 0.20) \times 10^{4}$	0.890
	35	$(4.15 \pm 0.52) \times 10^{-4}$	$(9.18 \pm 0.20) \times 10^{3}$	0.809
	45	$(4.12 \pm 0.73) \times 10^{-4}$	$(1.02 \pm 0.23) \times 10^{4}$	0.695

Table S2 shows that as the temperature rises, negative ΔG° values grow, indicating spontaneous adsorption. The positive ΔH° implies that the adsorption process is endothermic. Furthermore, this value (34.85 kJ/mol) within the 20–80 kJ/mol range indicates the effectiveness of electrostatic interactions in the adsorption process (Machado et al., 2012). A positive ΔS° value (0.222 kJ/mol) suggests raised randomness at the interface between the sorbate and solution during adsorption. This implies the possibility of structural modifications or rearrangements in the complex produced by the Sg@Aln and Ni^{2+} ions (Ho, 2003; Naseri et al., 2023).

3.7. Effect of ionic strength

Figure S4 shows the ionic strength effect on the Ni^{2+} adsorption performance of Sg@Aln. The adsorption capacity of Ni^{2+} dropped slightly from 46.06 mg/g to 43.01 mg/g due to the increased competition from background electrolyte ions. The impact of ionic strength on the Ni^{2+} ion uptake by Sg@Aln could provide proof of the mechanism of electrostatic interaction.

3.8. Column studies

Fig. 2a indicates the adsorption yield of Ni^{2+} ions in a fixed-bed column (10.5 mm internal diameter) filled with Sg@Aln as a function of the adsorbent amount. The adsorbent amount was changed from 20 to 90 mg at a 1.0 mL/min flow rate for Ni^{2+} solution of 100 mg/L. As the quantity of Sg@Aln increased, the adsorption yield of Sg@Aln increased progressively and then reached a saturation point. Higher quantities of adsorbent and a longer contact period between Ni^{2+} ions and Sg@Aln may account for this behavior. The removal percentage of Ni^{2+} reached 80.34% with 50 mg Sg@Aln, respectively.

The impact of flow rate on Ni^{2+} adsorption onto Sg@Aln is demonstrated in Fig. 2b. Increasing the flow rate of Ni^{2+} solution from 0.5 to 2.0 mL/min resulted in a slight reduction in the adsorption efficiency of Sg@Aln, from 80.47% to 70.58%. A nearly consistent adsorption performance was noted at higher flow rates. This could be explained by the fact that the Ni^{2+} ion solutions in the column had enough time to interact with Sg@Aln at the studied flow rates. 1 mL/min was chosen to make the adsorption process faster since at 0.5 and 1 mL/min almost the same adsorption performance of Sg@Aln was obtained.

Fig. 2c shows the breakthrough curve for Ni^{2+} removal onto Sg@Aln at a sorbent quantity of 50 mg, a sorbate concentration of 100 mg/L, and a constant flow rate of 1 mL/min. Following the adsorption process, Ni^{2+} analysis was conducted in the effluents. The fifteenth minute was the breakthrough point for Ni^{2+} removal. Saturation of the adsorbent occurred after 75 min.

The equilibrium adsorption capacity of the column (q_e, mg/g) at the saturation point (t_e, min) was calculated using Eq. (7). V_e represents the amount of Ni^{2+} that flowed downwards through the adsorption column (mL) till t_e, C_i and C_e represent the initial and final concentrations of Ni^{2+} (mg/L), respectively. m denotes Sg@Aln mass (g) employed in the adsorption column.

Eq. (8) can be employed to calculate the total Ni^{2+} solution volume. The adsorbed amount of Ni^{2+} (m_{ad}, g) onto Sg@Aln could be computed by Eq. (9). F denotes the flow rate (mL/min) (Aksu and Gönen, 2004).

$$q_e = \int_0^{V_e} \frac{C_i - C_e}{m} dV \tag{7}$$

$$V_e = F \times t_e \tag{8}$$

$$m_{ad} = \int_0^{V_e} (C_i - C_e)\, dV \tag{9}$$

Eqs. (10) and (11) (Aksu and Gönen, 2004) may also be utilized to ascertain the absolute percentage of treatment (R) and the mass transfer zone (Z_m), respectively, where H indicates the height of Sg@Aln in the

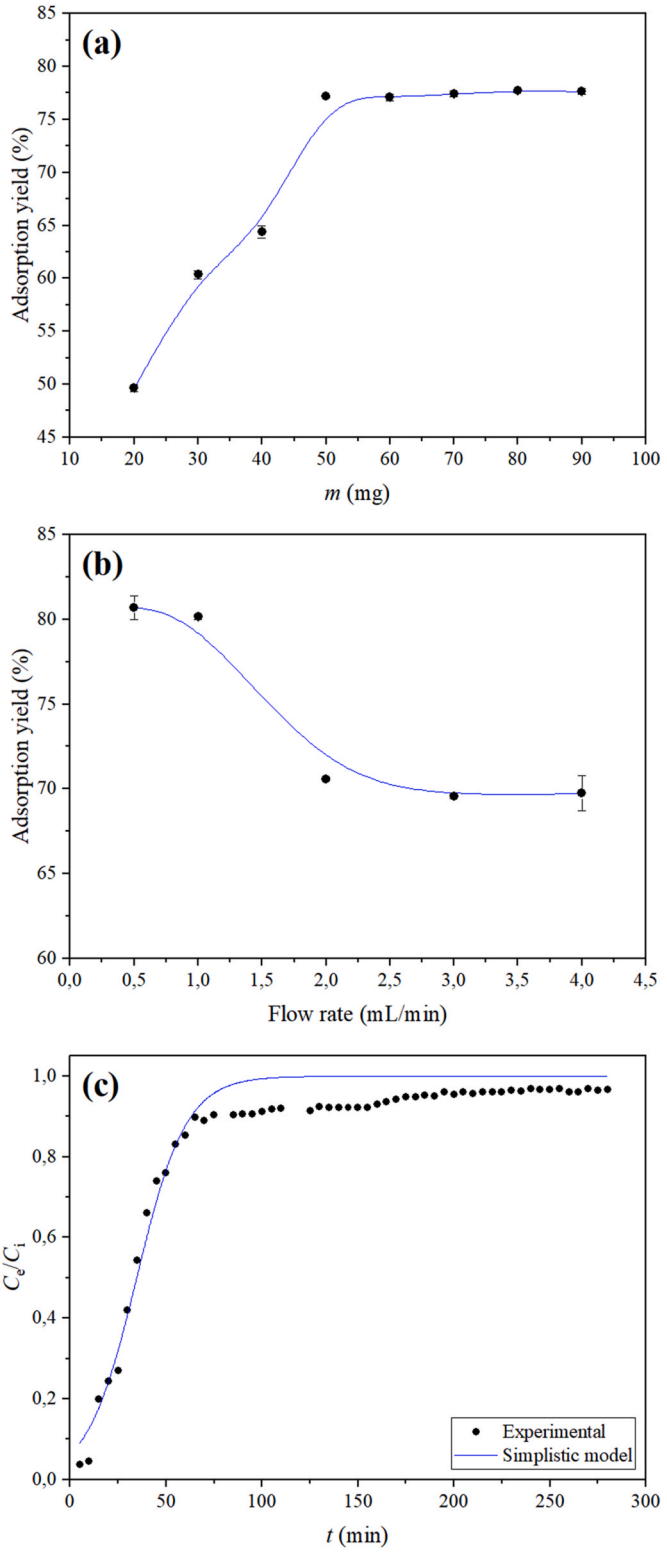

Fig. 2. Ni^{2+} adsorption onto Sg@Aln at different adsorbent doses (pH: 5.0, C_0: 100 mg/L, V: 25 mL, flow rate: 1 mL/min) **(a)** Ni^{2+} adsorption onto Sg@Aln at different flow rates (pH: 5.0, m: 50 mg, C_0: 100 mg/L, V: 25 mL, flow rate: 1 mL/min) **(b)** in column systems and breakthrough curve for Ni^{2+} adsorption onto Sg@Aln (pH: 5.0, m: 50 mg, C_0: 100 mg/L, flow rate: 1 mL/min) **(c)**.

column (cm).

$$R = \frac{m_{ad}}{C_i \times t_e \times F} \times 100000 \quad (10)$$

$$Z_m = H \times \left(1 - \frac{t_b}{t_e}\right) \quad (11)$$

The Bohart-Adams, Thomas, and Yoon-Nelson models are commonly applied for kinetic analysis in breakthrough curve modeling. Nevertheless, these models are similar and can be viewed as mathematically identical, as evidenced by the simplified equation (Eq. (12)) introduced by Chu (2020). The pertinent model parameters (a and b) are outlined in the supplementary materials (Table S3).

$$\frac{C_e}{C_i} = \frac{1}{1 + \exp(a - bt)} \quad (12)$$

The coefficients derived from this simplified equation are displayed in Table S4. The correlation coefficient ($r^2 = 0.950$) suggests that the experimental data correlated by this model. Saturation capacity values obtained from the breakthrough curve ($q_e = 73.53$ mg/g) and the Thomas model ($q_T = 69.35$ mg/g) suggest that Sg@Aln can be efficiently used in a fixed-bed column system. The experimental results (35 min) were consistent with Yoon-Nelson's τ value (34.7 min). All the results indicated that Sg@Aln exhibits excellent properties as a sorbent material for large-scale studies on removing Ni^{2+} ions from wastewater in a fixed-bed column system.

3.9. Real wastewater application

The yield of Sg@Aln's Ni^{2+} removal was tested in batch and column systems using real wastewater to evaluate the adsorbent's performance in real situations. Wastewater was supplied from a metal treatment unit of a plant in Eskişehir, Turkey. Metal ions content was analyzed by AAS and found as Na^{+}: 7.2 mg/L, K^{+}: 0.27 mg/L, Mg^{2+}: 2.22 mg/L, Ca^{2+}: 1.36 mg/L, Mn^{2+}: 0.017 mg/L, Cu^{2+}: 0.014 mg/L, Zn^{2+}: 0.009 mg/L, SO_4^{2-}: 19.14 mg/L, NO_3^{-}: 18.15 mg/L, Cl^{-}: 5.85 mg/L. The wastewater sample was spiked with 100 mg/L Ni^{2+}, and the optimum procedure (pH = 5.0) for adsorption was performed. The adsorption yields of Sg@Aln were 63.32% (q_e: 41.23 mg/g) and 49.84% (q_e: 33.20 mg/g) in real wastewater samples for batch and continuous systems, respectively. A slight decrease in the adsorption performance of Sg@Aln in real conditions may be attributed to a competition between target Ni^{2+} ions and the co-ions in the wastewater. These results also demonstrate that Sg@Aln could effectively treat heavy metal-ion-containing wastewaters with a comparatively high adsorption capacity.

3.10. Analysis of ANN for Ni^{2+} removal by Sg@Aln

Fig. 3a–h shows the regression plots of ANN output results vs. Ni^{2+} adsorption capacity of Sg@Aln in batch and column systems, respectively, for the training, validation, testing, and all prediction sets. In all cases, the ANN findings closely matched Sg@Aln's experimental Ni^{2+} removal capacity. As seen in Fig. 3d–h, the ANN model established a strong relationship with the training, validation, and testing data for batch-mode adsorption of Ni^{2+}. It also performed in column systems well in the training validation, while relatively well in the validation and testing despite some data scattering (Fig. 3f and g). As seen in (Fig. 3d and h), the ANN model performed overall with satisfactory results for both the batch and column adsorption experimental datasets. Additionally, lower MSE values (Table 3) indicate that an ANN model may be used to reliably estimate Ni^{2+} removal yields by Sg@Aln under specific batch and column conditions. In this context, we believe the outcomes of our investigation can potentially guide for future research on the identical application of the ANN model to other composite adsorbent systems.

3.11. Characterization

The FTIR spectra of Sg@Aln and Ni^{2+} loaded Sg@Aln are shown in Fig. 4a. Alunite's infrared spectrum shows a band at 3483 cm^{-1} in the

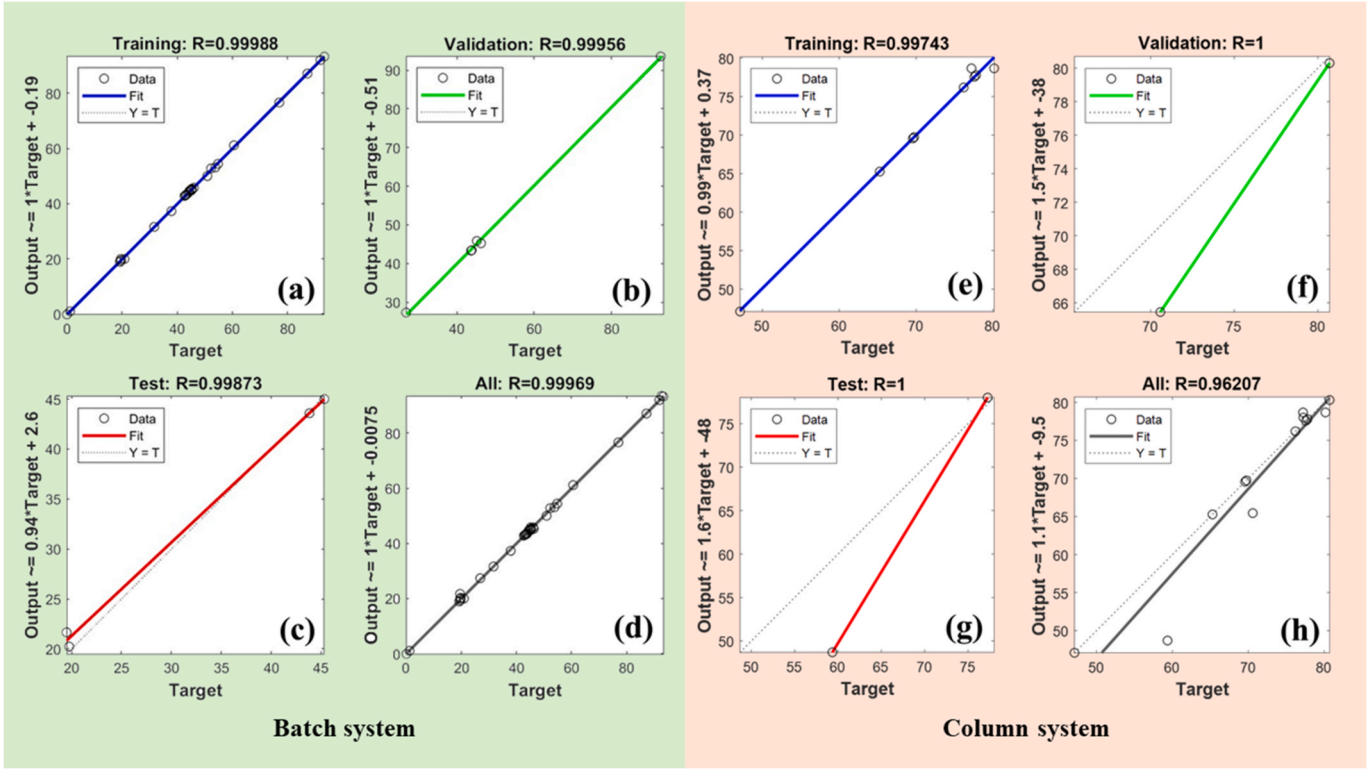

Fig. 3. ANN fitting regression plots for Ni^{2+} adsorption onto Sg@Aln in batch and column system.

Table 3
Values obtained by the ANN model for Ni^{2+} adsorption onto Sg@Aln

Parameters	Batch				Column			
	Training	Validation	Testing	All data	Training	Validation	Testing	All data
MSE	0.8149	0.7742	1.0053	0.8275	0.4835	13.264	56.961	11.138
R	0.9992	0.9992	0.9984	0.9991	0.9974	0.9999	1	0.9621

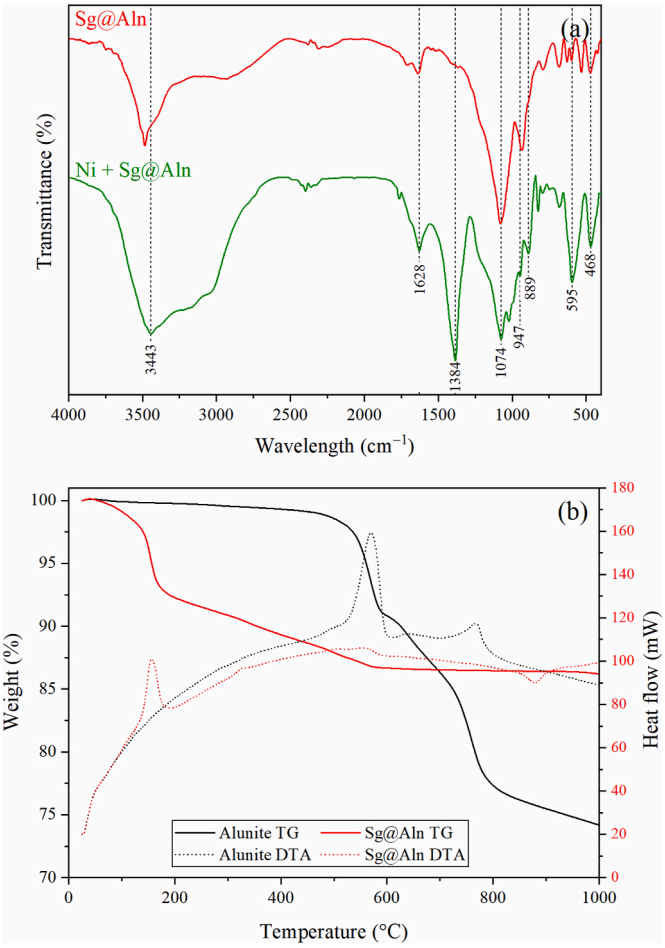

Fig. 4. FTIR spectra of Sg@Aln and Ni^{2+} loaded-Sg@Aln **(a)** DTA/TG curves of alunite and Sg@Aln **(b)**.

–OH stretching region. The weak peaks at 1638 and 1080 cm^{-1} can be assigned to O–H–O bending vibration of interlayer water and sulfate units, respectively. Two absorption bands at 620 and 680 cm^{-1} were due to the (SO_4^{2-}) bending vibrations. Band due to –OH bending vibrations in alunite is assigned at 600 cm^{-1} (Bishop and Murad, 2005; Frost and Wain, 2008; Tunali Akar et al., 2013). The intensities of the peaks at 1635 and 1080 cm^{-1} increased in the FTIR spectrum of Sg@Aln. This observed increase after silica-gel immobilization can be attributed to the overlap of the relevant groups with the Si–OH and Si–O–Si stretching vibrations originating from the silica-gel matrix (Antony et al., 2014). The peaks in the spectrum of Sg@Aln at around 793, 933, and 470 cm^{-1}, responding to the symmetrical stretching vibration of Si–O are other findings confirming the immobilization of the mineral with silica-gel (Li et al., 2021).

Following the nickel loading procedure, the absorption bands in Sg@Aln's spectrum at 3483, 1638, 1080, and 933 cm^{-1} shifted to 3443, 1628, 1074, and 947 cm^{-1}, respectively. These results demonstrated the potential role of these binding sites on Sg@Aln in the uptake process of nickel ions. Additionally, a distinct peak at 1384 cm^{-1} was observed in the spectrum of nickel ions loaded Sg@Aln, which can be explained by Si–O stretching vibration (Frost et al., 2008) or presence of nitrate. Moreover, peak intensities of the 468 and 595 cm^{-1} bands, which can be attributed to Ni–O, increased after the nickel uptake process, while the band at 889 cm^{-1}, which can also be attributed to Ni–O (Jabeen and Rafique, 2014; Iqbal et al., 2020; Moavi et al., 2021), stands out in the Sg@Aln's spectrum. All these observations give strong evidence that nickel ions interacted with the Sg@Aln surface.

Desulfurization and dehydroxylation are essential stages in the thermal decomposition of the alunite. Following an endothermic peak at 553 °C, the alunite undergoes desulphurization (Fig. 4b). During this stage, the mineral transformed into crystalline and amorphous alumina. The second endothermic peak at 750 °C indicates that alunite is partially desulfurized (Kashkai and Babaev, 1969; Tunali Akar et al., 2023).

Moisture loss caused an initial 1.5% mass decrease for Sg@Aln (Fig. 4b) at temperatures ranging from 25 to 120 °C. An endothermic peak in the DTA curve at 140 °C could be attributed to the structural arrangements in the silica network. The third continuous mass loss (~5.5%) in the TG curve between 200 and 580 °C could be due to the H-bonding of chemically sorbed water to silanol groups (Waseem et al., 2011). Additionally, it was evident that immobilized alunite had improved thermal stability.

SEM and EDX investigations were also performed to examine the surface morphology of alunite (Fig. S5a), Sg@Aln before (Fig. S5b) and after the Ni^{2+} ions were removed (Fig. S5c). Sg@Aln had a rough, disordered, and heterogeneous structure composed of a combination of particles of varied sizes before the Ni^{2+}removal. The surface of the material appeared denser due to the penetration of Ni^{2+} ions into Sg@Aln after the adsorption of Ni^{2+} ions. With SEM pictures alone, it was exceedingly challenging to determine whether Ni^{2+} ions adsorption took place. As a result, EDX analysis was used to identify the presence of Ni^{2+} ions on the surface of Sg@Aln. The EDX spectrum for Ni^{2+}-sorbed Sg@Aln (Fig. S5c) clearly shows the nickel peak at about 1 keV but the Sg@Aln EDX spectrum (Fig. S5b) does not display the characteristic peak for Ni^{2+} ions.

The specific surface area of Sg@Aln is 1.46 m^2/g and the total pore volume was 2.23 × 10^{-3} cm^3/g. The average pore diameter was calculated as 3.06 nm. Based on these findings, it can be concluded that the prepared adsorbent has primarily mesoporous (2–50 nm) structure. The N_2 adsorption/desorption isotherms for Sg@Aln are given in Fig. S6. The IUPAC classification reveals that the N_2 adsorption isotherm of Sg@Aln is categorized as Type III (Donohue and Aranovich, 1998).

All investigations demonstrated that complexation, electrostatic interaction, and pore filling were the most important mechanisms in Ni^{2+} adsorption with Sg@Aln. It was determined that –OH, Si–OH, Si–O–Si, and Si–O groups could potentially be effective in the adsorption process (Fig. S7).

4. Conclusion

This study demonstrated that it is possible to design a new composite based on alunite mineral doped with silica gel that could potentially be used as an effective and durable adsorbent for the removal of Ni^{2+} ions from a contaminated aqueous medium. The predictive ANN model was found to be successful in generating precise predictions of Ni^{2+} ion uptake within the range for which it was trained in both batch and continuous modes. Modeling the impacts of process variables using an

ANN tool can increase process performance and enable scaling up, lowering the cost of wastewater treatment operations. Another significant benefit in terms of process economy is the extremely short equilibrium time. The adsorption process was best represented using the Langmuir isotherm model. Consequently, the adsorption process can be considered to involve monolayers with similar but slightly different adsorption site energies. The initial pH and adsorbent quantity influenced Sg@Aln's adsorption efficacy for Ni^{2+} ions. The pseudo-second-order kinetic model regulated the Ni^{2+} elimination process. Thermodynamic data suggested endothermicity, spontaneity, and adsorption favorability. The practical use of Sg@Aln in real wastewater allows it to be used for metal removal. Overall, the present achievement improves ecosystem health, economic growth and environmental protection. It can be concluded that Sg@Aln is a remarkable adsorbent capable of efficiently removing nickel ions from water and using a simple synthesis process. Given its encouraging outcomes, it is recommended that Sg@Aln's efficacy be tested on other types of contaminants.

CRediT authorship contribution statement

Sibel Tunali Akar: Writing – original draft, Supervision, Resources, Methodology, Formal analysis, Conceptualization. **Suzan Rüstemoğlu:** Investigation. **Serpil Turkyilmaz:** Methodology, Formal analysis, Data curation. **Fatih Sayin:** Visualization, Formal analysis. **Tamer Akar:** Writing – review & editing, Resources, Formal analysis.

Funding

This research did not receive any specific grant from funding agencies in the public, commercial, or not-for-profit sectors.

Declaration of competing interest

The authors declare that they have no known competing financial interests or personal relationships that could have appeared to influence the work reported in this paper.

Appendix A. Supplementary data

Supplementary data to this article can be found online at https://doi.org/10.1016/j.chemosphere.2025.144127.

Data availability

No data was used for the research described in the article.

References

Ahmad Aftab, R., Zaidi, S., Aslam Parwaz Khan, A., Arish Usman, M., Khan, A.Y., Tariq Saeed Chani, M., Asiri, A.M., 2023. Removal of Congo red from water by adsorption onto activated carbon derived from waste black cardamom peels and machine learning modeling. Alexandria Eng. J. 71, 355–369.

Ahmaruzzaman, M., 2011. Industrial wastes as low-cost potential adsorbents for the treatment of wastewater laden with heavy metals. Adv. Colloid Interface Sci. 166, 36–59.

Akar, T., Celik, S., Gorgulu Ari, A., Tunali Akar, S., 2013. Nickel removal characteristics of an immobilized macro fungus: equilibrium, kinetic and mechanism analysis of the biosorption. J. Chem. Technol. Biotechnol. 88, 680–689.

Aksu, Z., Gönen, F., 2004. Biosorption of phenol by immobilized activated sludge in a continuous packed bed: prediction of breakthrough curves. Process Biochem 39, 599–613.

Alahabadi, A., Singh, P., Raizada, P., Anastopoulos, I., Sivamani, S., Dotto, G.L., Landarani, M., Ivanets, A., Kyzas, G.Z., Hosseini-Bandegharaei, A., 2020. Activated carbon from wood wastes for the removal of uranium and thorium ions through modification with mineral acid. Colloids Surf. Physicochem. Eng. Aspects 607, 125516.

Ali, H., Khan, E., Ilahi, I., 2019. Environmental chemistry and ecotoxicology of hazardous heavy metals: environmental persistence, toxicity, and bioaccumulation. J. Chem. 2019, 6730305.

Amin, K.F., Gulshan, F., Asrafuzzaman, F.N.U., Das, H., Rashid, R., Manjura Hoque, S., 2023. Synthesis of mesoporous silica and chitosan-coated magnetite nanoparticles for heavy metal adsorption from wastewater. Environ. Nanotechnol. Monit. Manage. 20, 100801.

Anastopoulos, I., Pashalidis, I., Hosseini-Bandegharaei, A., Giannakoudakis, D.A., Robalds, A., Usman, M., Escudero, L.B., Zhou, Y., Colmenares, J.C., Núñez-Delgado, A., Lima, É.C., 2019. Agricultural biomass/waste as adsorbents for toxic metal decontamination of aqueous solutions. J. Mol. Liq. 295, 111684.

Antony, R., David Manickam, S.T., Kollu, P., Chandrasekar, P.V., Karuppasamy, K., Balakumar, S., 2014. Highly dispersed Cu(II), Co(II) and Ni(II) catalysts covalently immobilized on imine-modified silica for cyclohexane oxidation with hydrogen peroxide. RSC Adv. 4, 24820–24830.

Bilal, M., Ihsanullah, I., Younas, M., Ul Hassan Shah, M., 2021. Recent advances in applications of low-cost adsorbents for the removal of heavy metals from water: a critical review. Sep. Purif. Technol. 278, 119510.

Bishop, J.L., Murad, E., 2005. The visible and infrared spectral properties of jarosite and alunite. Am. Mineral. 90, 1100–1107.

Bosacka, A., Zienkiewicz-Strzałka, M., Deryło-Marczewska, A., Chrzanowska, A., Wasilewska, M., Sternik, D., 2022. Physicochemical, structural, and adsorption properties of chemically and thermally modified activated carbons. Colloids Surf. Physicochem. Eng. Aspects 647, 129130.

Boyd, G.E., Adamson, A.W., Myers, L.S., 1947. The exchange adsorption of ions from aqueous solutions by organic zeolites. II. Kinetics1. J. Am. Chem. Soc. 69, 2836–2848.

Choi, M.-Y., Kang, J.-K., Lee, C.-G., Park, S.-J., 2022. Feasibility of fluoride removal using calcined *Mactra veneriformis* shells: adsorption mechanism and optimization study using RSM and ANN. Chem. Eng. Res. Des. 188, 1042–1053.

Chu, K.H., 2020. Breakthrough curve analysis by simplistic models of fixed bed adsorption: in defense of the century-old Bohart-Adams model. Chem. Eng. J. 380, 122513.

Denkhaus, E., Salnikow, K., 2002. Nickel essentiality, toxicity, and carcinogenicity. Crit. Rev. Oncol./Hematol. 42, 35–56.

Dharmarathna, S.P., Priyantha, N., 2024. Investigation of boundary layer effect of intra-particle diffusion on methylene blue adsorption on activated carbon. Energy Nexus 14, 100294.

Donohue, M.D., Aranovich, G.L., 1998. Classification of Gibbs adsorption isotherms. Adv. Colloid Interface Sci. 76–77, 137–152.

Dubinin, M.M., Radushkevich, L.V., 1947. The equation of the characteristic curve of activated charcoal. Proceedings of the Academy of Sciences, Physical Chemistry Section 55, 331–333.

El-Naggar, A., Ahmed, N., Mosa, A., Niazi, N.K., Yousaf, B., Sharma, A., Sarkar, B., Cai, Y., Chang, S.X., 2021. Nickel in soil and water: sources, biogeochemistry, and remediation using biochar. J. Hazard Mater. 419, 126421.

Elovich, S.Y., Larinov, O.G., 1962. Theory of adsorption from solutions of non electrolytes on solid (I) equation adsorption from solutions and the analysis of its simplest form, (II) verification of the equation of adsorption isotherm from solutions. Izvestiya Akademii Nauk. SSSR, Otdelenie Khimicheskikh Nauk 2, 209–216.

Foroutan, R., Esmaeili, H., Abbasi, M., Rezakazemi, M., Mesbah, M., 2018. Adsorption behavior of Cu(II) and Co(II) using chemically modified marine algae. Environ. Technol. 39, 2792–2800.

Freundlich, H.M.F., 1906. Über die adsorption in lösungen. Z. Phys. Chem. 57, 385–470.

Frost, R.L., Jagannadha Reddy, B., Dickfos, M.J., 2008. Raman spectroscopy of the nickel silicate mineral pecoraite—an analogue of chrysotile (asbestos). J. Raman Spectrosc. 39, 909–913.

Frost, R.L., Wain, D., 2008. A thermogravimetric and infrared emission spectroscopic study of alunite. J. Therm. Anal. Calorim. 91, 267–274.

Genchi, G., Carocci, A., Lauria, G., Sinicropi, M.S., Catalano, A., 2020. Nickel: human health and environmental toxicology. Int. J. Env. Res. Public Health 17, 679.

Ghaedi, A.M., Vafaei, A., 2017. Applications of artificial neural networks for adsorption removal of dyes from aqueous solution: a review. Adv. Colloid Interface Sci. 245, 20–39.

Ho, Y.-S., 2003. Removal of copper ions from aqueous solution by tree fern. Water Res. 37, 2323–2330.

Ho, Y.S., McKay, G., 1999. Pseudo-second order model for sorption processes. Process Biochem. 34, 451–465.

Iqbal, J., Abbasi, B.A., Ahmad, R., Mahmoodi, M., Munir, A., Zahra, S.A., Shahbaz, A., Shaukat, M., Kanwal, S., Uddin, S., Mahmood, T., Capasso, R., 2020. Phytogenic synthesis of nickel oxide nanoparticles (NiO) using fresh leaves extract of *Rhamnus triquetra* (wall.) and investigation of its multiple in vitro biological potentials. Biomedicines 8, 117.

Jabeen, B., Rafique, U., 2014. Synthesis and application of metal doped silica particles for adsorptive desulphurization of fuels. Environ. Eng. Res. 19, 205–214.

Kalantari, A., Kamsin, A., Shamshirband, S., Gani, A., Alinejad-Rokny, H., Chronopoulos, A.T., 2018. Computational intelligence approaches for classification of medical data: state-of-the-art, future challenges and research directions. Neurocomputing 276, 2–22.

Kashkai, M.A., Babaev, I.A., 1969. Thermal investigations on alunite and its mixtures with quartz and dickite. Mineral. Mag. 37, 128–134.

Kasprzak, K.S., Sunderman, F.W., Salnikow, K., 2003. Nickel carcinogenesis. Mutat. Res., Fundam. Mol. Mech. Mutagen. 533, 67–97.

Lagergren, S., 1889. Zur theorie der sogenannten adsorption gelöster stoffe. Kungliga Svenska Vetenskapsakademiens Handlingar 24, 1–39.

Langmuir, I., 1918. The adsorption of gases on plane surfaces of glass, mica and platinum. J. Am. Chem. Soc. 40, 1361–1403.

Li, C., Zhao, J., Zhang, Y., 2021. Study on adsorption behavior of nickel ions using silica-based sandwich layered zirconium-titanium phosphate prepared by layer-by-layer grafting method. Nanomaterials 11, 2314.

López, A., Lázaro, N., Marqués, A.M., 1997. The interphase technique: a simple method of cell immobilization in gel-beads. J. Microbiol. Methods 30, 231–234.
Lima, E.C., Hosseini-Bandegharaei, A., Moreno-Piraján, J.C., Anastopoulos, I., 2019. A critical review of the estimation of the thermodynamic parameters on adsorption equilibria. Wrong use of equilibrium constant in the Van't Hoff equation for calculation of thermodynamic parameters of adsorption. J. Mol. Liq. 273, 425–434.
Machado, F.M., Bergmann, C.P., Lima, E.C., Royer, B., de Souza, F.E., Jauris, I.M., Calvete, T., Fagan, S.B., 2012. Adsorption of Reactive Blue 4 dye from water solutions by carbon nanotubes: experiment and theory. Phys. Chem. Chem. Phys. 14, 11139–11153.
Mandal, S., Mahapatra, S.S., Sahu, M.K., Patel, R.K., 2015. Artificial neural network modelling of As(III) removal from water by novel hybrid material. Process Saf. Environ. Prot. 93, 249–264.
Moavi, J., Buazar, F., Sayahi, M.H., 2021. Algal magnetic nickel oxide nanocatalyst in accelerated synthesis of pyridopyrimidine derivatives. Sci. Rep. 11, 6296.
Mondal, M.I.H., Chandra Chakraborty, S., Rahman, M.S., Marjuban, S.M.H., Ahmed, F., Zhou, J.L., Ahmed, M.B., Zargar, M., 2024. Adsorbents from rice husk and shrimp shell for effective removal of heavy metals and reactive dyes in water. Environ. Pollut. 346, 123637.
Naseri, A., Abed, Z., Rajabi, M., Lal, B., Asghari, A., Baigenzhenov, O., Arghavani-Beydokhti, S., Hosseini-Bandegharaei, A., 2023. Use of Chrysosporium/carbon nanotubes for preconcentration of ultra-trace cadmium levels from various samples after extensive studies on its adsorption properties. Chemosphere 335, 139168.
Natrayan, L., Arul Kumar, P.V., Dhanraj, J.A., Kaliappan, S., Sivakumar, N.S., Patil, P.P., Sekar, S., Paramasivam, P., 2022. Synthesis and analysis of impregnation on activated carbon in multiwalled carbon nanotube for Cu adsorption from wastewater. Bioinorg. Chem. Appl. 2022, 7470263.
Raninga, M., Mudgal, A., Patel, V.K., Patel, J., Kumar Sinha, M., 2023. Modification of activated carbon-based adsorbent for removal of industrial dyes and heavy metals: a review. Mater. Today: Proc. 77, 286–294.
Raval, N.P., Shah, P.U., Shah, N.K., 2016. Adsorptive removal of nickel(II) ions from aqueous environment: a review. J. Environ. Manage. 179, 1–20.
Shahryari, T., Singh, P., Raizada, P., Davidyants, A., Thangavelu, L., Sivamani, S., Naseri, A., Vahidipour, F., Ivanets, A., Hosseini-Bandegharaei, A., 2022. Adsorption properties of Danthron-impregnated carbon nanotubes and their usage for solid phase extraction of heavy metal ions. Colloids Surf. Physicochem. Eng. Aspects 641, 128528.
Sivasankar, V., Rajkumar, S., Murugesh, S., Darchen, A., 2012. Influence of shaking or stirring dynamic methods in the defluoridation behavior of activated tamarind fruit shell carbon. Chem. Eng. J. 197, 162–172.
Tomczak, E., 2011. Application of ANN and EA for description of metal ions sorption on chitosan foamed structure—equilibrium and dynamics of packed column. Comput. Chem. Eng. 35, 226–235.
Tripathi, A., Ranjan, M.R., 2015. Heavy metal removal from wastewater using low cost adsorbents. J Bioremed Biodeg 6, 1000315.
Tunali Akar, S., Alp, T., Yilmazer, D., 2013. Enhanced adsorption of Acid Red 88 by an excellent adsorbent prepared from alunite. J. Chem. Technol. Biotechnol. 88, 293–304.
Tunali Akar, S., Tunc, D., Sayin, F., Akar, T., 2023. Chitosan functionalized alunite as a green composite for sorption and preconcentration of copper: from parametric optimization to application. J. Polym. Environ. 31, 1359–1372.
Vinayagam, R., Nagendran, V., Goveas, L.C., Narasimhan, M.K., Varadavenkatesan, T., Samanth, A., Selvaraj, R., 2024. Machine learning, conventional and statistical physics modeling of 2,4-Dichlorophenoxyacetic acid (2,4-D) herbicide removal using biochar prepared from Vateria indica fruit biomass. Chemosphere 350, 141130.
Volesky, B., 2001. Detoxification of metal-bearing effluents: biosorption for the next century. Hydrometallurgy 59, 203–216.
Waseem, M., Mustafa, S., Naeem, A., Shah, K.H., Shah, I., 2011. Mechanism of Cd (II) sorption on silica synthesized by sol–gel method. Chem. Eng. J. 169, 78–83.
Weber, W.J., Morris, J.C., 1963. Kinetics of adsorption on carbon from solution. J. Sanit. Eng. Div. 89, 31–60.
WHO, 2022. Guidelines for Drinking-Water Quality: Fourth Edition Incorporating the First and Second Addenda. World Health Organization, Geneva. https://www.ncbi.nlm.nih.gov/books/NBK579460/table/ch12.tab105/.
Yousefi, M., Akbari, H., Adibzadeh, A., Mohammadi, A.A., Baziar, M., Abbasi Farajzadeh, M., Akbari, H., 2024. Adsorption of diazinon from aqueous solution using metal organic framework and functionalized graphene: comparison of BBD. ANN models. Chemosphere 351, 141222.
Zhang, L., Yang, L., Yang, M., You, X., Hong, Y., Yang, Y., Chen, J., Lin, Y., Zhang, Y., Zhou, X., 2024. Phosphorus recovery from urine by CO_2-activated biochar for sustainable slow-release fertilizer applications: unveiling adsorption mechanisms by statistical physics modeling and predictive modeling with artificial neural networks. Sep. Purif. Technol. 342, 126981.